MMW-Scanning Radar for Descent Guidance and Landing Safeguard

Alex Foessel-Bunting and William Whittaker
Robotics Institute, Carnegie Mellon University, Pittsburgh, PA 15213-3890, USA
{afoessel,red}@cmu.edu

Keywords: spacecraft safety, millimeter-wave radar, altimetry, terrain mapping, descent guidance.

Abstract

This paper explores the use of millimeter-wave (MMW) scanning radar for control and safeguarding during spacecraft descent and landing. The essay compares radar characteristics such as beam width, agility and range accuracy, against sensing requirements for a specific descent and landing scenario. While the study discussed here presents the advantages of agile motion-free scanning radar for mapping the landing area and providing altimetry and velocity, it also examines radar shortcomings, such as wide beam, and poor range resolution. The conclusions guide the design of a radar interpreter to alleviate these shortcomings and to generate, maintain and refine a terrain map during the descent and landing stages. Such terrain models could provide the necessary information to guide a landing spacecraft away from the dangers of scientifically interesting areas onto a safe landing site.

1 Introduction

Current radar altimeters provide information on spacecraft velocity, altitude and attitude for descent and landing control through the use of fixed-antenna beams. However, radar altimeters fall short of providing robust terrain profiling, which can be useful for real time descent guidance and safety as well as for subsequent surface vehicle deployment. Radar altimeters are unable to rapidly measure adjacent points for construction of a contour. Profile information becomes more critical as missions attempt landings on geologically interesting areas. This is because the diversity of terrain features endangers spacecraft that use current blind landing techniques.

There are ongoing efforts to use descent visual imagery for the creation of high-accuracy terrain elevation maps of the landing site area [1]. Initial maps of a landing site area are critical for the performance of autonomous rover localization and navigation in future space missions. Descent visual imagery is also a tool for coordinating rovers in a robotic colony, for site selection, and as a precursor to human exploration. Attempts have been made [2] to use the imagery for control of the descent trajectory and selection of the landing site as the lander approaches the surface. The investigation proposes early detection and tracking of the landing site to guide the spacecraft and reduce the size of the uncertainty ellipse. Another approach uses laser ranging and detection for terrain mapping and hazard detection [3]. However, the efficacy of these approaches is greatly hindered by windstorms that create dusty surface conditions and that challenge the use of visual imagery for descent and landing ranging.

Narrow-beam scanning MMW radar can provide terrain contour data for descent and landing control of spacecraft under all conditions, thus lifting weather and cloud restrictions for planetary landing [4]. As the descent progresses, the radar detects smaller features and could help to guide the spacecraft to a safe and appropriate landing site. Even when landing is imminent, radar can easily penetrate airborne dust created by the landing thrust and can continuously provide control inputs.

Motion-free beam steering is especially attractive because of its reliability advantages as well as because of its ability to permit rapid and gross changes in beam direction which enables flexible scan patterns and fast steer to specific points of interest [5]. However, the adoption of motion-free electronic techniques to steer a radar beam introduces additional complexities due to variable beam characteristics throughout the scan pattern. For instance, at extreme scanning angles the mainlobe widens. Also the sidelobes have reduced attenuation with respect to the mainlobe. Additional shortcomings of radar include specular reflections with certain natural materials as well as a rather wide beam angle.

Software interpretation techniques somewhat overcome these shortcomings in light of these various beam characteristics. One technique that has been used with other sensing modalities is the compilation of successive scan data from different locations into a composite image, which reduces overall data uncertainty. In addition, a sensor model that captures the varying antenna-radiation pattern can compensate for the varying sidelobes. The resolution of the radar

increases as the lander descends and decreased cell size allows the representation of smaller features in the areas of interest. The use of inertial information can help to reduce the processing costs related to the subsequent images registration. Despite radar shortcomings, scene models could be created with vast improvement over what is possible by the mapping of raw-signal data.

2 Related Work

This section revises the landing selection criteria and highlights the conflicting objectives of exploring geologically interesting sites and maintaining high standards in spacecraft safety. The section also shows how the information provided by new sensors orbiting Mars assists in the selection process. Nevertheless the descent and landing uncertainty still translates into high risk landings suggesting the need for real-time hazard detection and safeguarding. Initiatives are in place to use optical ranging sensors for hazard detection, but Mars dust storms could blind those optical sensor and pose a threat to the descent and landing phases. This section also includes a description of current radar use in spacecraft descent and landing control. It also describes the limitations of current altimeters, which prevent their use for hazard detection.

2.1 Landing Site Selection

Unmanned spacecraft have commonly landed blindly. For instance the largest risk taken during the Viking lander design was the landing site selection. The engineers discovered that current imagery did not provide sufficient knowledge of small-scale features on the surface to guarantee the absence of hazards [6]. Posterior analyses of Viking landing sites indicates that the landing risk was larger than the initial assessment.

Improvements have been made in the available information for site selection. The Pathfinder mission used the imagery from the Viking orbiters. A major difference between the landing site selection process for the next Mars lander and that of Pathfinder is the availability of new information from the completed Pathfinder mission and the ongoing Mars Global Surveyor (MGS) mission. The high-resolution Mars Orbiter Camera (MOC) images will be required on any approved landing site or on nearby similar terrain. The reason for this is that MOC images show omnipresent sand dunes where few or none exist on the Viking scale images. Slip faces on sand dunes are at or near the angle of repose, which is well beyond the 10 degree slope limit safety for the lander. Also, the elevation will be provided by the Mars Orbiter Laser Altimeter (MOLA) and requiring delay-Doppler radar data would severely reduce the number of possible sites.

Despite the advances in quality and coverage of images from the surface of Mars, landings are far from being safe and certain because another reason exists for why blind landings are dangerous: the landing site uncertainty of current spacecraft descent trajectories.

2.2 Landing Ellipse

Current unmanned spacecraft landing techniques do not allow for precision landing. The landing area instead defined by an ellipse with a major axis parallel to the pre-descent orbital direction. This ellipsis typically is 200-km long and 30-km wide around the targeted site because of uncertainties in navigation and atmospheric entry. Ongoing research efforts intend to reduce the size of the uncertain area.

Even optimistic expectations predict that the uncertain landing area will continue to be several square kilometers over the next years. The only data points we have today are the landings of the two Viking landers and the landing of the Pathfinder. In the case of the Vikings, they landed 29 and 6 km from the intended landing sites. Pathfinder landed approximately 22 km away from the target site [7]. In the case of this latest lander, the ellipse center and size changed over time. The ellipse size in fact decreased to a mere 15 km by 8.4 km four hours before landing, and the spacecraft landed 5 km from the center of this reduced ellipse.

Despite improvements in spacecraft-position estimation, the level of precision is far from sufficient for hazard avoidance. This means that site selection must again be based on a large area free from hazards. The entire uncertain landing ellipse must be free of steep slopes, scarps and obvious hazards, must have acceptable radar reflectivity, and moderate rock abundance and must have little or no dust.

Under these criteria, engineers select the landing sites in areas devoid of known dangers and features. These sites tend not to appeal the scientists because they would rather have landing sites in geographically interesting areas.

2.3 Real-Time Hazard Detection

Landing counterexamples with small level of uncertainty exist, such as the manned Apollo missions. In those cases, a pilot guided the spacecraft to a safe landing site. In other words, Apollo spacecraft had an active real-time hazard avoidance system: the pilot. Unfortunately this will not be the case for a Mars spacecraft for several years. Still is possible real-time hazard avoidance if a way exists to detect the hazards in time to maneuver and avoid them.

The concept of using real-time hazard detection has been explored for a number of sensors. Polzleitner

and Paar proposed the use of computer vision for early identification of a target landing site and subsequent tracking for spacecraft guidance [2]. The proposed method matches images taken during the descent phase with a database of all orbital imagery contained int the uncertainty ellipse. This method also recommends preselection of landmarks for simpler computing.

A more recent investigation proposes the use of LIDAR (LIght Detection And Ranging) for hazard avoidance [3]. The work presents a simulation tool to evaluate the sensor requirements and to support mission design. Also, the investigation presents preliminary analysis and concludes with approval of the performance of the methods for hazard detection. The study focuses on a LIDAR sensor, which is the baseline for the Mars 2007 Smart Lander mission. The LIDAR has two gimbal-mounted mirrors that sweep the beam across the field of view.

Both approaches address real-time hazard detection and can provide information to the spacecraft control so that it can maneuver and avoid hazardous areas. However, these studies do not consider dust or storms that blind visible light sensors.

2.4 Dust and Storms

Yet another challenge for precise landing on Mars is the presence of an atmosphere that can lift and hold dust and sand. Different from that of the Moon where dust and sand rise and fall immediately following ballistics trajectories, the Martian atmosphere has winds and the extended presence of flying particles. Mars is famous for large, planet-wide dust storms.

The data provided by the Mars Global Surveyor show large storms of sand and dust. Such storms are common on Mars in the spring, when sublimation of the frozen carbon dioxide that caps the planet's poles boosts the planet's atmospheric pressure, allowing it to hold on to more dust for longer periods. In addition, sharp temperature contrasts between different color areas give rise to strong winds on Mars. This can initiate dust storms that often envelop the entire planet.

Storms and winds are not the only sources of flying dust and sand. The profile of the Viking II mission describes the effect of bad timing in the control of landing thrusters. Because radar misidentification of a rock or a highly reflective surface, the thrusters fired an extra 0.4 seconds before landing—cracking the surface and raising dust.

2.5 Altimetry and Radar Altimeters

Spacecraft such as the Mars Polar Lander are equipped with a radar altimeter designed to let the craft know its altitude as it plummets toward the surface. The information is used to control the pulsing action of a dozen rocket thrusters that will slow the craft down as it nears the surface. The Pathfinder mission used a radar altimeter that was activated following heat shield release. The specified altimeter maximum range was 1,520 m. The radar altimeter operated in a "first-return mode," transmitting a series of radar pulses to the surface and clocking the time to the first received signal. Altitude data were provided with 0.3-m resolution at a frequency of 50 Hz. The mass of the radar altimeter was 1.4 kg.

Although most radar altimeters provide altimetry for landing control, there are studies to use altimeters to provide surface terrain maps. One such study proposes using a radar altimeter to build reflectivity maps of the Martian surface and, as a secondary science objective, to produce topographic maps [8]. However such topographic maps result from many observations and from the averaging of several readings. No such mapping would be possible from a descending spacecraft, and no hazard detection would result.

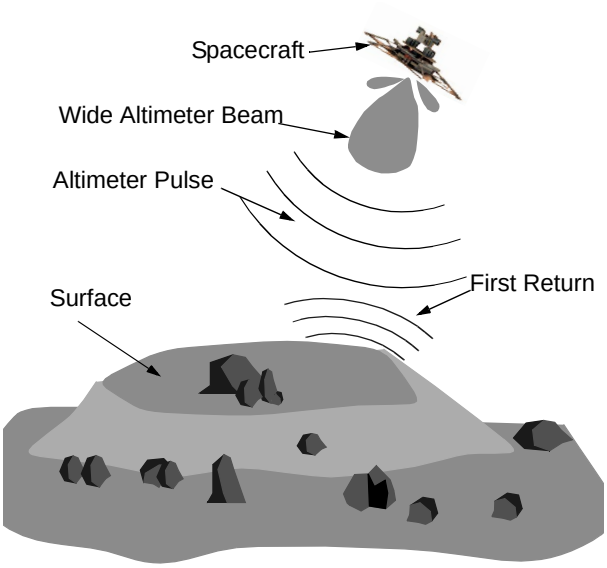

Fig. 1. Spacecraft using an altimeter to control the descent. This spacecraft is unable to avoid hazards because the altimeter only provides a distance to the closest large reflecting surface.

The lack of cross range resolution is a feature of descent radar altimeters. This prevents detection of hazards. Radar altimeters transmit a beam several tens of degrees wide, which produces a large footprint on the surface. This wide beam is necessary to compensate for nonhorizontal attitudes. The echo typically reflects from the center of mass of the footprint, and all small objects and slopes disappear in the main echo. Figure 1 shows the use of a radar altimeter to control the descent.

3 Scanning Radar Approach

This paper studies the use of narrow-beam MMW radar to increase the spacecraft safety through the descent and landing phases. The approach focuses on early detection of obstacles using scanning radar to enable avoidance maneuvering. A description of the sensor and an indication of the characteristics that make it appropriate for the hazard detection task follow this section introduction. The section later outlines the hazard detection and altimetry requirements based on the previously described landing scenario and compares the sensor capabilities to the requirements. The section also studies the surface representation requirements to integrate the radar observations.

3.1 Scanning Radar

A scanning radar operates on the same principle as radar altimeters to measure range from the sensor to the surface. However it uses a narrow beam to estimate range to a reduced spot on the surface. Figure 2 shows the radar steering the narrow beam to cover the entire field of view, which is typically several tens of degrees in both axes. The accumulation of this series of observations shapes a terrain map suitable for hazard detection and maneuvering planning.

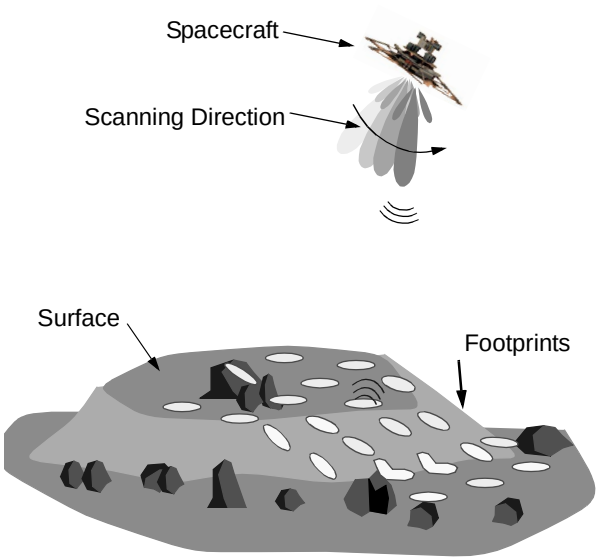

Fig. 2. Spacecraft mapping the surface during descent with a scanning radar. The radar antenna sequentially aims a narrow beam towards the surface. The radar calculates the distance and builds a terrain map.

Angular resolution is the result of low beam divergence (i.e., a narrow beam). The beamwidth is inversely proportional to antenna aperture for a given frequency. For commercial applications, 77 GHz is a common MMW-radar frequency. A 1° beam is achieved with an antenna aperture of 224 mm at that frequency. This applies to both axes in the case of a symmetrical beam defining minimum width and height for the antenna. Achieving a narrower beam requires an impractical antenna size for spacecraft applications. Therefore the angular resolution for point targets is limited.

Although they provide encouraging data, existing millimeter-wave radar devices require moving parts to scan the radar beam and are thus large and heavy. If the size, weight and power requirements of the sensor can be decreased, the potential for application to a variety of space tasks is enormous. Reliability also plays an important role in space applications where any interruption in the operation compromises mission success. In general moving parts are less reliable than their fixed counterparts, so a completely solid state scanning radar should greatly improve the dependability and ultimately the space readiness. In addition, motion-free beam steering is especially attractive due to its ability to permit rapid gross changes in beam direction enabling flexible scan patterns and fast pointing to specific points of interest.

3.2 Motion-Free Scanning Radar

There are several technologies that achieve motion-free scanning: phased-array antennas and reconfigurable-plasma refraction antennas are two examples.

In comparison to common phased-array beam steering approaches, which are complex and expensive, reconfigurable-plasma diffraction antennas offer an alternate approach to electronic beam steering that promises to be much less expensive, more compact and lightweight. One such technology is an optically controlled two-axis scanning antenna. The antenna employs a photo-conducting wafer in which a spatially varying plasma density is photo-injected by a LED array source. The varying plasma density alters the local dielectric constant of the wafer material and allows diffractive control over incident MMW radiation [5].

Figure 3 shows two reflector configurations. Note the center of the concentric rings or Fresnel zones. The beam steering angle is related to the position of the concentric rings on the reflector. This type of antenna is also known as a Soret-reflector antenna. The reconfigurable plasma shapes in concentric rings known as Fresnel zones.

Current design specify the ability to reconfigure the plasma for a new beam orientation in less than 50 µs. Nevertheless, the radar operates with a frequency-modulated continuous-wave (FMCW) transceiver. This class of transceivers has a minimum time of operation of 200 µs. The combination of the motion-free scanning antenna and the FMCW transceiver achieves 4,000 observations per second. A full frame is the scan of the entire field of view of 60° by 60° at steps

of 2° for complete coverage. A full frame acquisition takes less than 0.25 s. If the radar uses narrower beam of 1°, a full frame acquisition takes approximately 1 s.

This study relates the descent-guidance and landing-safeguarding requirements with the performance of a motion-free scanning radar prototype, which can shape a 2° beam and steer it in a ±30° angular range in elevation and azimuth using a frequency of 77 GHz and a 0.15-m diameter antenna. An antenna aperture twice as large would shape a 1° beam. The motion-free nature of the scanning system enables the selection of random and discontinuous scan patterns, suggesting oversampling techniques to improve resolution.

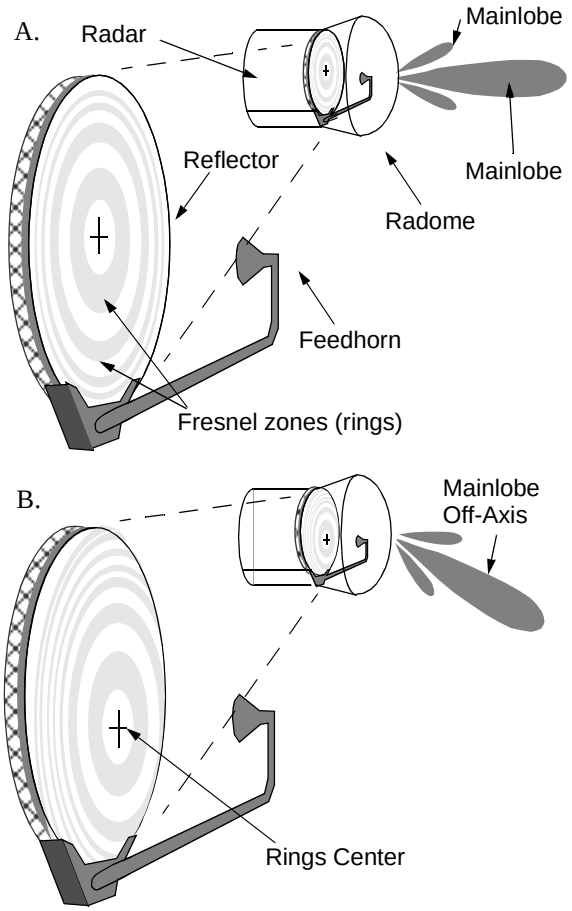

Fig. 3. A motion-free scanning antenna operates using a dynamic Soret lens. The patterns in the reflector shape a beam according to the center of the concentric rings. Reflector A points the mainlobe straight ahead. Reflector B points downward and to the right of the antenna. Note the cross in the center of the rings en each reflector.

3.3 Mars Descent Profile

A summary of typical Mars landing mission detection requirements follows. The descent profile is extracted from the Mars Polar Lander plans [9]. Table I presents data of the planned descent trajectory.

After the orbit insertion, the spacecraft reduces its speed by adopting an attitude with the heat shield towards the direction of motion and uses the atmosphere to slow down. When the speed reaches acceptable levels, a parachute reduces the speed further. When the spacecraft speed is too slow for the parachute to be effective, a mechanism jettisons the parachute and the landing rockets control the descent until landing. Because the spacecraft still has horizontal speed remaining, the attitude remains in the direction of motion. This stage is the "flare." The non horizontal attitude has implications in radar altimetry and imaging because the attitude of the spacecraft dramatically changes the field of view for the optical and ranging sensor.

TABLE I: DESCENT SCENARIO

Event	Time	Altitude	Horiz.	Speed	Angle[a]
	(sec.)	(m)	(m)	(m/s)	(deg)
Heatshield jettison	110	7,500.	5,400	230	54
	100	6,700	4,300	136	47
	90	5,900	3,450	116	38
	80	5,000	2,750	114	36
	70	4,100	2,100	111	32
	60	3,300	1,600	94	29
	50	2,500	1,150	91	30
Lander separation	40	1,800	750	80	30
Powered descent	30	1,200	400	69	23
	20	600	150	65	13
	10	260	70	34	15
Hovering	3	10	2	5	11
Landing	0	0	0	3	0

a. This is the trajectory angle with respect to vertical motion.

3.4 Detection Requirements

The detection requirements for a safeguarding and guidance sensor that operates during descent and landing fall in three coverage scales: global, regional and local [10]. Each scale has an associated altitude range.

Global scale relates to altitudes from 6,000 m to 2,000 m above the planetary surface. At this altitude, the spacecraft should detect large terrain features that can jeopardize the mission. Examples of those features are: escarpments, hills, and steep slopes. The spacecraft has time to detect these features and to plan the descent trajectory into more favorable areas.

The regional scale considers altitudes from 2,000 m to 500 m. At this point, the sensor should detect craters larger than 10 m in diameter and deeper than 2 m, as well as slopes steeper than 30°.

Spacecraft maneuvering is limited during the global and regional altitude ranges because it is under parachute control. Also the spacecraft attitude is mostly determined by the parachute braking action.

The local scale ranges from 500 m to 40 m. The sensor should detect and resolve cylinder-like objects with 20-cm diameter and 50-cm length, and slopes steeper than 10°. The spacecraft has now jettisoned the parachute and has the capability to maneuver based on the hazard detection performed previously.

3.5 Altimetry Requirements

Imaging requirements imply that the sensor has to measure the range to the surface. Nevertheless, spacecraft descent control and landing have specific altimetry requirements [10]. The sensor should estimate altitude within one meter below 3,000 m and 7.5 cm below 500 meters. The requirements of horizontal- and vertical-velocity accuracy are 0.1 to 0.2 m/s at altitudes as low as 2,000 m. The descent velocity measurement rate required increases to one hertz rate below 500 m.

4 Calculations and Discussions

4.1 Beam Divergence

The beam diverges with distance. The footprint is the area covered by a single beam. This area depends on the beamwidth and the range from the sensor to the surface. Table II presents the footprint size at different altitudes for a 2° and 1° beams. The calculations assume a horizontal spacecraft.

TABLE II: FOOTPRINT SIZE AND COVERAGE

Scale	Altitude (m)	FOV[a] (m)	Footprint		Requirements	
			2° Beam (m)	1° Beam (m)	Obstacle (m)	Slope (°)
Global	5,900	6,812	206	103	--	--
Global	5,000	5,773	174	87	--	--
Global	4,100	4,734	143	71	--	--
Global	3,300	3,810	115	57	--	--
Global	2,500	2,886	87	43	--	--
Regional	1,800	2,078	62	31	10[b]	30
Regional	1,200	1,385	41	20	10	30
Regional	600	692	20	10	10	30
Local	260	300	9	4	0.5[c]	10
Local	10	11	0.3	0.2	0.5	10
Local	0	0	0	0	0.5	10

a. The field of view assumes 60° scanning in both axes.
b. This refers to the detection of craters of given diameter.
c. This refers to the detection of objects of a given size.

The footprint size defines the cross range resolution and the ability to detect small targets. This is critical for the detection of negative obstacles such as craters. The detection requirements specify detection of 10-m diameter craters in the Regional scale altitude range.

A 1° beam achieves a 10-m footprint at an altitude of approximately 600 m. The 2° beam achieves the same footprint size at 300 m. These results indicate that the smaller antenna does not satisfy the detection of 10-m diameter craters in the Regional scale; the larger antenna marginally does.

The detection of slopes does not present a challenge to either antenna because the radar down range resolution is better than 0.5 m. A slope of 30° over an extension of 10-m presents an altitude variation of 5 m, which is easily detected by the radar. Similarly, a slope of 10° that extends over 5 m has an altitude variation of 0.9 m. This variation is also detected by the radar.

A larger antenna aperture can shape a narrower beam. Future research plans to develop a second generation sensor with an antenna with an aperture of 30 cm, twice the aperture of the current development. This antenna will generate footprints half the size. Higher radar frequencies also result in narrower beams. Higher frequencies would require a complete new design at potentially high cost. The developments at frequencies over 100 GHz are limited.

4.2 Attitude, Altitude and Coverage

Because the objective of the radar is the detection of hazards previous to landing, the study seeks to evaluate if the sensor has the landing site within its field of view. The field of view is 60° in both axes. Figure 4 shows the case when the landing site is within the field of view. This figure shows a spacecraft attitude almost tangential to the trajectory. Commonly the spacecraft is a more horizontal attitude.

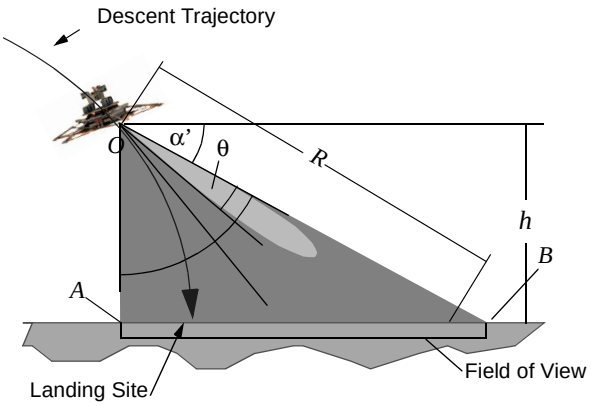

Fig. 4. Scheme of the field of view for the radar given the spacecraft attitude and altitude. It is important that the field of view includes the landing site. The figure also shows a beam and the resulting footprint.

After the parachute deployment, when the braking effect is maximum, the attitude of the spacecraft is very close to the angle of the trajectory. In this case the axis of the radar is aiming in the trajectory direction, as it is shown in Figure 4. Once the parachute approaches a constant speed, the attitude becomes horizontal and the radar axis points more downwards.

Since the descent scenario does not provide spacecraft attitude, the coverage study must rest on an estimation of the attitude. Table III presents two scenarios: one using the trajectory angle as the spacecraft attitude, and the other using a horizontal attitude throughout the descent. The column heading notation "Side A" and "Side B" is consistent with the notation of Figure 4. If the side A is negative and B positive, the landing site is in the field of view. If both values are positive, the landing site falls out of the field of view. In this condition the sensor fails to detect hazards in the landing site.

TABLE III: RADAR COVERAGE OF LANDING SITE

Altitude (m)	Horizontal (m)	Angle (°)	0°		Angle	
			Side A (m)	Side B (m)	Side A (m)	Side B (m)
5,900	3,450	38	500	6400	-2016	2642
5,000	2,750	36	250	5250	-1812	2241
4,100	2,100	32	50	4150	-1520	1957
3,300	1,600	29	-50	3250	-1239	1637
2,500	1,150	30	-100	2400	-1009	1161
1,800	750	30	-150	1650	-813	742
1,200	400	23	-200	1000	-554	554
600	150	13	-150	450	-261	323
260	70	15	-60	200	-114	137
10	2	2	-3	7	-3	7
0	0	0	0	0	0	0

The table shows altitudes with the landing site out of the field of view (Side A and side B positives). This is the case when the attitude is horizontal, but only for the higher altitudes where the spacecraft is likely inclined.

When the attitude is horizontal, the landing site is permanently within the field of view. These results indicate that a 60° field of view suffices for the detection of hazards in the intended landing site.

4.3 Speed Effects on Radar

Radar energy propagates at the speed of light. When the antenna generates a pulse from a moving platform, two phenomena can occur: radial or downrange speed induces a Doppler shift in the range estimation, and tangential or cross-range speed induces losses because the motion situates the antenna in a lower gain zone. The Doppler shift is easily compensated in FMCW radars with the use of a triangular modulation.

An estimation of the time of flight for the altitude range of interest gives a maximum of 0.6 µs. If the speed is 500 m/s, the translation is 30 mm, which is insignificant.

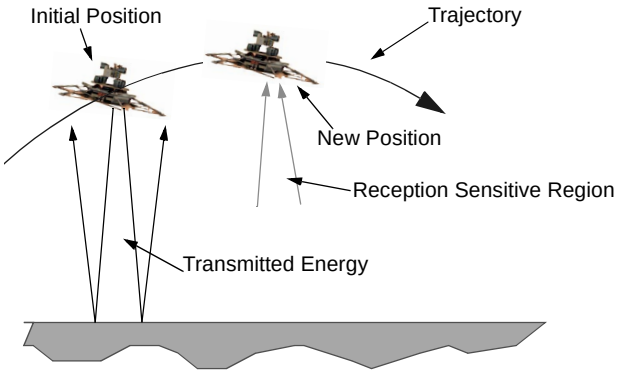

Fig. 5. The motion of the spacecraft can produce degradation in the radar because the motion over the trajectory situates the sensor in a position off the main antenna gain. Calculations show this effect is non important.

4.4 Radar Data Integration

Figure 6 presents a combination of observations taken from two nearby vantage points. The altitude over the surface is the same for the two vantage points. The horizontal distance is small. The dashed line shows a more accurate resulting terrain profile. The surface profile more accurately reflects the actual surface. The combination of observations from a sequence of vantages points further improves the model quality.

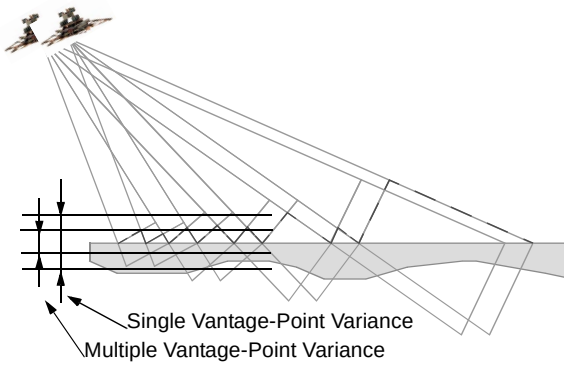

Fig. 6. The combination of observations from different position in the spacecraft trajectory can improve the fidelity of terrain maps. In this particular case, a flat surface appears flatter and the sensor has reduced false alarms.

As opposed to land applications that require full three-dimensional models to represent overhanging obstacles, descent and landing application only requires a 2½-D representation. Previous work has investigated a full three-dimensional volumetric representation for ground vehicle applications [11]. This tessellated representation consists of a value per cell that represents the log of the odds of the existence of a solid body in the cell.

The planetary landing case is different because the scenario is amenable to some simplifications and assumptions. Spacecraft safety suggests that most proposed landing sites will be flat. Also no hazards exist in the atmosphere. Therefore the representation should be just enough to represent the surface and the small variations due to craters, river beds and other features.

5 Conclusion and Future Work

This essay has explored the use of MMW motion-free scanning radar for control and safeguarding of descent and control of a Mars lander. A sensor capable of providing real-time hazard detection through a dusty environment such as Mars atmosphere can make a vast difference in the level of safety of a spacecraft that lands on Mars. The motion-free scanning nature of the sensor makes it a preferred sensor for space applications. It is also a sensor that could sustain long hovering periods close to the surface because it is immune to the dust produced by the thrusters.

The study concludes that the beamwidth is marginally sufficient to satisfy the crater detection in the regional area. The down range resolution is appropriate for slope detection. The sensor field of view is sufficiently wide and does not constraint the spacecraft attitude. Only in the unlikely case of a horizontal attitude after parachute deployment, the landing site is not within the sensor field of view.

The same study opens more issues such as the spacecraft fuel budget design. Today conservative estimates consider enough fuel to reduce the speed and guarantee a safe landing plus a safety margin. Future designs will have to balance the hazard avoidance capabilities of the spacecraft with the additional fuel for hovering.

Another open area of investigation is the allocation of the radar observations. Since the radar does not have to follow any mechanically constrained scanning pattern, the radar can focus most observations on a particular area of interest and build a high quality map faster.

Finally, this line of research has impact on in-space operations and on surface systems: Motion-free scanning radar and rapid radar interpretation and terrain map building can enable in-descent landing area and landing site evaluation, thus increasing safety and flexibility in lander operations (unmanned and manned). Additional applications include safeguarding and terrain avoidance for aerial robotic systems (e.g., aerial surface sampling systems), as well as providing terrain maps for subsequent surface vehicle deployment.

References

[1] Larry H. Matthies, Clark F. Olson, Greg Tharp, and Sharon Laubach, “Visual Localization Methods for Mars Rovers Using Lander, Rover, and Descent Imagery,” *Proc. of the 4th Int. Symp. on Artificial Intelligence, Robotics and Automation in Space*, Tokyo, Japan, 1997.

[2] W. Polzleitner and G. Paar, “Surface Relative Spacecraft Navigation using Computer Vision,” *SPIE Vol. 2352, Mobile Robots IX*, 1994.

[3] A. Johnson, A. Klumpp, J. Collier and A. Wolf, “Lidar-based Hazard Avoidance for Safe Landing on Mars,” *AAS/AIAA Space Flight Mechanics Meeting*, February 2001.

[4] A. Foessel, S. Chedda, D. Apostolopoulos, “Short-Range Millimeter-Wave Radar Perception in a Polar Environment,” *Proc. Int. Conf. on Field and Service Robots (FSR'99)*, Pittsburgh, Pennsylvania, August 1999.

[5] G. Webb, S. Rose, M. Sanchez, J. Osterwalder, “Experiments on an Optically Controlled 2-D Scanning Antenna”, *Proceedings of the 1998 Antenna Applications Symposium, Monticello-Illinois.*

[6] I. Taback and J. Goodlette, “The Viking Lander—Then and Now,” *Mars: Past, Present and Future, Progress in Astronautics and Aeronautics*, Vol. 145, 1992.

[7] D. Spencer et al, “Mars Pathfinder Atmospheric Entry Reconstruction,” AAS Technical Report 98-146

[8] C. Federico, G. Picardi, R. Seu, “A conceptual radar system to perform reflectivity and topographic maps of the Martian surface,” *Proc. CIE Int. Conf. Radar*, Rome University., Italy, 1996.

[9] NASA/JPL/MSSS, “Mars Polar Lander Descent Imaging: Two Minutes of Work,” http://mars.jpl.nasa.gov/msp98/msss/mardi_hardware/descent/

[10] D. Smith, “Sensor Delta Review,” Unpublished meeting presentation slides, Jet Propulsion Laboratory, January 2000.

[11] A. Foessel-Bunting, “Radar Sensor Model for Three Dimensional Map Building,” *Proc. SPIE, Mobile Robots XV and Telemanipulator and Telepresence Technologies VII*, SPIE, Vol. 4195, November, 2000.